ResearchGate

See discussions, stats, and author profiles for this publication at: https://www.researchgate.net/publication/49761315

Decomposition of excited electronic state s-tetrazine and its energetic derivatives

ARTICLE *in* THE JOURNAL OF CHEMICAL PHYSICS · JANUARY 2011

Impact Factor: 2.95 · DOI: 10.1063/1.3523649 · Source: PubMed

CITATIONS
10

READS
53

3 AUTHORS, INCLUDING:

Atanu Bhattacharya
Indian Institute of Science
20 PUBLICATIONS **275** CITATIONS
SEE PROFILE

Elliot R Bernstein
Colorado State University
317 PUBLICATIONS **6,961** CITATIONS
SEE PROFILE

Available from: Elliot R Bernstein
Retrieved on: 20 January 2016

Decomposition of excited electronic state s-tetrazine and its energetic derivatives

Yuanqing Guo, Atanu Bhattacharya, and Elliot R. Bernstein[a)]
Department of Chemistry, NSF ERC for Extreme Ultraviolet Science and Technology, Colorado State University, Fort Collins, Colorado 80523-1872, USA

(Received 3 September 2010; accepted 12 November 2010; published online 12 January 2011)

Decomposition of excited electronic state s-tetrazine and its energetic derivatives, such as 3-amino-6-chloro-1,2,4,5-tetrazine-2,4-dioxide (ACTO), and 3,3′-azobis (6-amino-1,2,4,5-tetrazine)-mixed N-oxides ($DAATO_{3.5}$), is investigated through laser excitation and resonance enhanced multi photon ionization techniques. The N_2 molecule is detected as an initial product of the s-tetrazine decomposition reaction, through its two photon, resonance absorption transitions [$a''\ ^1\Sigma_g^+$ ($v' = 0$) $\leftarrow X\ ^1\Sigma_g^+$ ($v'' = 0$)]. The suggested mechanism for this reaction is a concerted triple dissociation yielding rotationally cold (~20 K) ground electronic state N_2 and 2 HCN molecules. The comparable decomposition of excited electronic state ACTO and $DAATO_{3.5}$ yields an NO product with a cold rotational (~20 K) but a hot vibrational (~1200 K) distribution. Thus, tetrazine and its substituted energetic materials ACTO and $DAATO_{3.5}$ evidence different decomposition mechanisms upon electronic excitation. N_2O is excluded as a potential intermediate precursor of the NO product observed from these two s-tetrazine derivatives through direct determination of its decomposition behavior. Calculations at the CASMP2/CASSCF level of theory predict a concerted triple dissociation mechanism for generation of the N_2 product from s-tetrazine, and a ring contraction mechanism for the generation of the NO product from the energetic s-tetrazine derivatives. Relaxation from S_n evolves through a series of conical intersections to S_0, upon which surface the dissociation occurs in both mechanisms. This work demonstrates that the substituents on the tetrazine ring change the characteristics of the potential energy surfaces of the derivatives, and lead to a completely different decomposition pathway from s-tetrazine itself. Moreover, the N_2 molecule can be excluded as an initial product from decomposition of these excited electronic state energetic materials. © *2011 American Institute of Physics*. [doi:10.1063/1.3523649]

I. INTRODUCTION

As one of the most important building blocks of high nitrogen content compounds, s-tetrazine has been of great interest to chemists for over one century with regard to its spectroscopy[1–6] and photochemistry.[7–10] Due to its relatively high symmetry (D_{2h}) and its readily accessible visible and ultraviolet electronic transitions, the dissociative photochemistry of tetrazine has been a topic of considerable interest, both experimentally and theoretically.[11–13] Based on the observed initial dissociation products, such as HCN and N_2 from photo decomposition of s-tetrazine, and the calculated transition states, two major different dissociation mechanisms have been proposed:[13–15] 1) a concerted triple dissociation, and 2) a stepwise process. More detailed descriptions of these two mechanisms can be found in the study by Zhao *et al.*,[10] which employs a photofragment-translational spectroscopy method to study the photochemistry of s-tetrazine and confirm that s-tetrazine decomposes into $2HCN + N_2$ via a concerted triple dissociation mechanism.

However, the internal energy distributions of the N_2 product have, to date, not been reported. As one knows from studies of other energetic systems,[16–18] a detailed rotational and vibrational state distribution of the dissociation product(s) provides very important information for the determination of the decomposition mechanism. Thus, in the present study, the N_2 product from the photodecomposition of s-tetrazine is detected by a (2+1) resonance enhanced multi photon ionization (REMPI) method, by which the rotational distribution of the N_2 product, via its two photon resonance absorption transitions [$a''\ ^1\Sigma_g^+$ ($v' = 0$) $\leftarrow X\ ^1\Sigma_g^+$($v'' = 0$)] at 202 nm, can be determined. Based on the experimental measurements and theoretical calculations, a dissociation pathway for the decomposition of photo excited s-tetrazine at 202 nm can be determined (e.g., $S_n \rightarrow$ products, $S_n \rightarrow S_0 \rightarrow$ products, $S_n \rightarrow S_m \rightarrow S_0 \rightarrow$ products, etc.).

The tetrazine energetic derivatives 3-amino-6-chloro-1,2,4,5-tetrazine-2,4-dioxide (ACTO), and 3,3′-azobis (6-amino-1,2,4,5-tetrazine)-mixed N-oxides ($DAATO_{3.5}$) are two tetrazine-N-oxide based, high nitrogen content, energetic materials: they have recently received increased attention due in large part to their extremely high burn rate with low sensitivity to pressure.[19,20] The structures of these two molecules are characterized by a tetrazine-2,4-dioxide moiety (shown in Fig. 1), and the average oxygen content in DAATO is determined to be about 3.5 atoms per molecule.[21] Only a few studies of the basic sensitivity and performance

a)Author to whom correspondence should be addressed. Electronic mail: erb@lamar.colostate.edu.

 © 2011 American Institute of Physics

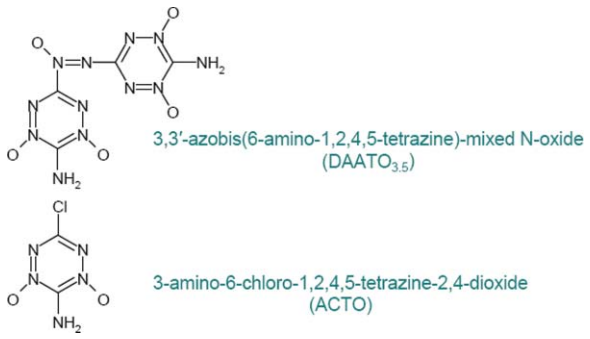

FIG. 1. Chemical structures of tetrazine energetic derivatives.

of these tetrazine-N-oxide based energetic materials have appeared in literature:[19,20] the decomposition mechanism of these molecules (especially following photo excitation) as energetic systems has not been well studied. Due to the similarity of the molecular structure of s-tetrazine, DAATO, and ACTO, one can easily think that ACTO and DAATO might experience a similar decomposition pathway to that of s-tetrazine, and the immediate discernible photodissociation product from these two molecules might be N_2O (see Fig. 2). N_2O can further dissociate into N_2 and NO as secondary decomposition products. N_2 and NO products have been detected from the excited electronic state decomposition of N_2O at 203 and 226 nm excitations, respectively. Comparisons of the decomposition products, and their internal energy distributions, from photodissociation of N_2O, ACTO, and $DAATO_{3.5}$ can determine whether N_2O is an initial product from the decomposition of excited electronic state ACTO and DAATO. The N_2 molecule is not observed from the decomposition of ACTO and DAATO at 203 nm excitation. Instead, the NO molecule is detected to be a decomposition product from both energetic molecules with rotational and vibrational distributions very different from the NO product from N_2O decomposition.[22] Thus, the N_2O molecule can be excluded as the initial decomposition product from these

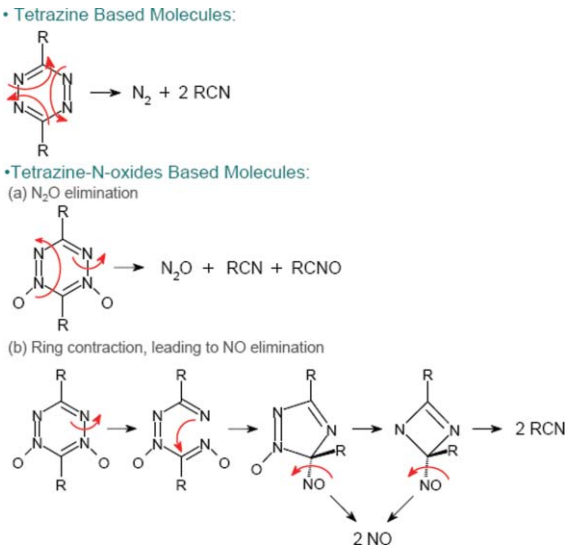

FIG. 2. Different possible decomposition pathways of tetrazine and its energetic derivatives.

tetrazine energetic derivatives. This work demonstrates that substituent groups on the tetrazine ring change the characteristics of the potential energy surfaces of the derivatives and that the tetrazine energetic derivatives decompose through a different mechanism than tetrazine itself.

Ab initio calculations at the CASMP2/CASSCF level of theory are employed to explore the relevant excited electronic state potential energy surfaces and conical intersections for s-tetrazine and ACTO. Based on these calculations and our experimental observations, we are able to determine the dissociation mechanisms for both tetrazine and its energetic derivatives, and describe and account for the differences between them.

II. EXPERIMENTAL PROCEDURES

The experimental apparatus used for photo excitation and the REMPI detection scheme is described in detail in our previous publications.[17–19] It consists of a supersonic jet expansion pulsed nozzle, a time-of-flight mass spectrometry (TOFMS) chamber, and nanosecond laser systems. In this work, a single pump/probe laser beam with eight ns pulse duration at different wavelengths (202, 226, 236, and 248 nm) is used both to initiate the dissociation of the molecules of interest and to detect decomposition products, such as N_2 [$a''\,^1\Sigma_g^+$ ($v' = 0$) $\leftarrow X\,^1\Sigma_g^+$ ($v'' = 0$) transitions at 202 nm] and NO [$A\,^2\Sigma^+$ ($v' = 0$) $\leftarrow X\,^2\Pi(v'' = 0,1,2)$ transitions at 226, 236 and 248 nm], by the REMPI technique. The tunable 202 nm laser wavelength is the third harmonic of a pulsed dye laser, pumped by the second harmonic (532 nm) of a neodymium-doped yttrium aluminum garnet laser's fundamental output (1.064 μm). The dye laser output is frequency doubled in a potassium dihydrogen phosphate (KDP) crystal and then frequency tripled in a BBO crystal.[23] The other three UV laser wavelengths are generated by the same dye laser in conjunction with a nonlinear wavelength extension system. Typical pulse energy of the UV laser beam is 200–600 μJ/pulse depending on the exact wavelength of interest for a one-color experiment. The laser intensity (I) is $\sim$1.3 to 4×10^7 W/cm^2 for an 8 ns laser pulse at a focused beam diameter of 0.5 mm.

The s-tetrazine sample is freshly synthesized before each experiment using s-tetrazine dicarboxylic acid sodium salt (Tiger Scientific), and the method described by Spencer *et al.*[2] The sample is stored in a glass vial and heated to about 60 °C. Gas phase molecules are brought into the expansion nozzle by He carrier gas. ACTO and $DAATO_{3.5}$ are supplied by Los Alamos National Laboratory (D. E. Chavez) and used without additional purification. The isolated gas phase ACTO and $DAATO_{3.5}$ are produced through a combination of matrix assisted laser desorption (MALD) and supersonic jet expansion described in detail elsewhere.[18,19] A 1% N_2O in He gas mixture is prepared for the calibration of N_2 and NO from decomposition of excited electronic state N_2O at the excitation wavelength mentioned above.

The experiment is run at a repetition rate of ten Hz. The timing sequence for the pulsed nozzle, ablation laser, and excitation/ionization laser is controlled by a time delay generator (SRS DG535). The molecular beam is perpendicularly crossed by the UV laser beam that is focused to a spot size of

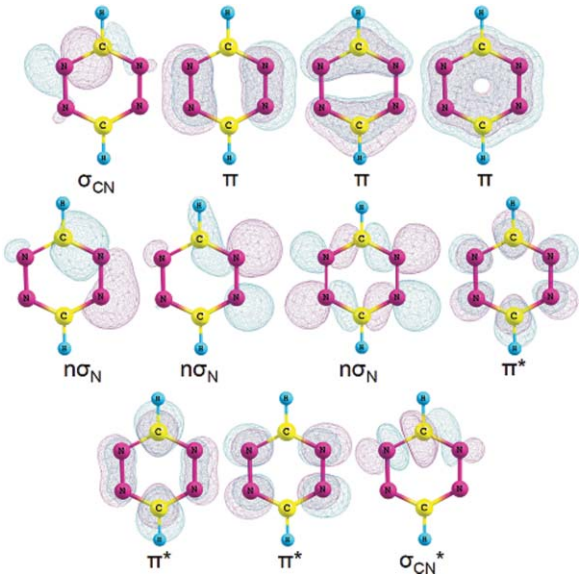

FIG. 3. Orbitals used in the active space of CASSCF calculations for s-tetrazine. The (14, 11) active space includes three bonding π, three antibonding π^*, three nonbonding $n\sigma_N$, one bonding σ_{CN}, and one antibonding σ_{CN}^*.

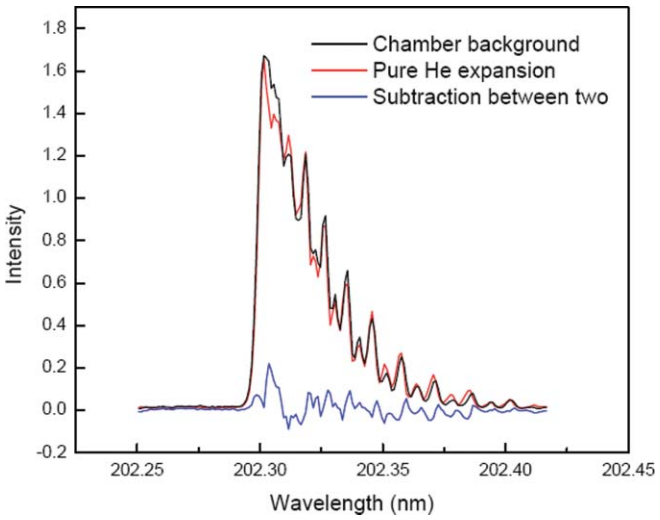

FIG. 4. $(2 + 1)$ REMPI spectrum of N_2 from background inside the vacuum chamber at 202 nm. Rotational temperature simulations with a Boltzmann population distribution show that the background N_2 inside the chamber has a rotational temperature of ca. 300 K. Thus the N_2 detected is not from the nozzle or its feed lines.

0.5 mm at the ionization region of the TOFMS. A background pressure of 1×10^{-5} Torr is maintained in the vacuum chamber during the experiment. Ion signals are detected by a microchannel plate detector. Signals are recorded and processed on a personal computer using a box car average (SRS SR 250) and an analogue to digital conversion card.

III. THEORETICAL METHODS

Potential energy surface calculations, search for conical intersections, and geometry optimizations for s-tetrazine and ACTO are performed at the CASSCF/6–31G(d) level of theory with the GAUSSIAN03 program.[24] Symmetry restrictions are not imposed for the calculations. For calculations of the excited state potential energy surface of s-tetrazine, an active space comprising 14 electrons in 11 orbitals, denoted as CASSCF (14, 11) is used. Orbitals used in the CASSCF (14, 11) calculations are three bonding π, three antibonding π^*, three nonbonding $n\sigma_N$, one bonding $n\sigma_{CN}$, and one antibonding $n\sigma_{CN}^*$, which are shown in Fig. 3. Detailed active space and orbital selection for the calculations of the excited state potential energy surfaces of ACTO can be found in our previous publication,[22] in which a maximum active space of CASSCF (14, 10) including bonding π, antibonding π^*, and two nonbonding orbitals, are employed. Vertical excitation energies are computed by state averaging over the ground state and two successive singlet excited states with equal weights. For reliable estimation of vertical excitation energies, MP2 correlated CASSCF energies are also calculated. Transition state structures are characterized by analytical frequency calculations. The selections of the level of theory and the active space are justified by the comparison between the calculated vertical excitation energies and experimental absorption maxima in Sec. V. The accuracies of the calculations along the reaction pathway are difficult to estimate since experimental information about the conical intersections and the transition states is not available. Calculations presented here, however, are based on the experimental observations, including decomposition products and the internal energy distributions within these products, and therefore the proposed reaction pathways based on the computational results provide a reasonable and qualitative interpretation to the experimental observations.

IV. EXPERIMENTAL RESULTS

Due to the high detection sensitivity of the REMPI technique, a background signal of the N_2 molecule inside the chamber under a pressure of 5×10^{-7} Torr is observed. The $(2 + 1)$ REMPI spectra of the background N_2 molecule are shown in Fig. 4. The black and red lines in this figure indicate the signal of N_2 inside the chamber without nozzle opening and with pure He carrier gas expansion, respectively; the blue noisy line indicates the subtraction between these two spectra. Apparently, the residual N_2 molecules inside the chamber contribute the major background signal, and any contribution from the He expansion gas/nozzle system can be neglected. The background spectrum exhibits well-resolved rotational structure up to J'' greater than 20 of the N_2 molecule. Based on a Boltzmann population distribution (T) and two-photon transition line strengths,[25] a rotational temperature of $\sim$300 K is found for the residual N_2 molecules inside the chamber, as to be expected. Since the background N_2 molecules do produce a relatively intense signal, extra care is taken to measure the N_2 products from the decomposition of systems of interest. For example, if a system produces an N_2 product with a similar rotational distribution to, or a colder distribution than the background N_2 molecules, the absorption spectra of the N_2 molecules from two different sources will overlap with one another. In this case, the background signal must be subtracted from the overlapping, summed spectra to

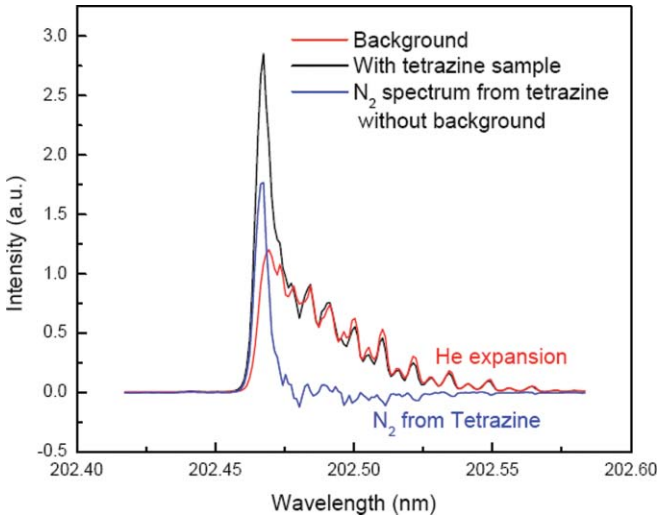

FIG. 5. (2 + 1) REMPI spectrum of N_2 from decomposition of excited electronic state s-tetrazine at 202 nm. Due to the overlap between background signal and N_2 from s-tetrazine, the net spectrum of N_2 from s-tetrazine is the difference between the signal with tetrazine sample and the background. Rotational temperature simulations with a Boltzmann population distribution show that the N_2 product from s-tetrazine has a rotational temperature of ca. 20 K.

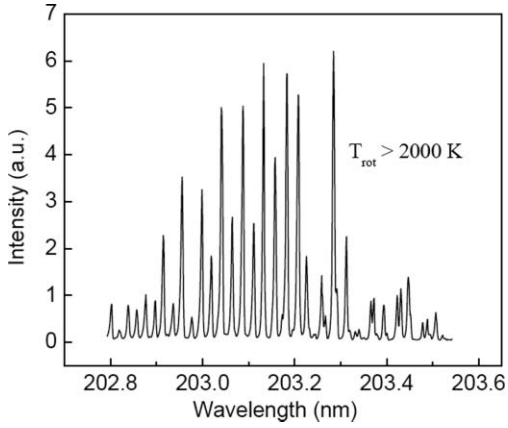

FIG. 6. (2 + 1) REMPI spectrum of N_2 from decomposition of excited electronic state N_2O at 203 nm. Rotational temperature simulations with a Boltzmann population distribution show that the N_2 product from N_2O gas has a rotational temperature of ca. 2000 K.

obtain the signal for the N_2 product from the decomposition process. On the other hand, if the N_2 product from decomposition has a rotational distribution much hotter than that of the background N_2 molecules, the absorption of the N_2 product will red shift away from the background N_2 molecules. This shift leads to a good separation of the spectra for the N_2 molecules from two different sources. These two different situations will be demonstrated below for the N_2 product detection from s-tetrazine and N_2O gas, respectively.

Figure 5 illustrates the (2 + 1) REMPI spectra of N_2 product from decomposition of excited electronic state s-tetrazine following single photon excitation at 202 nm. The black line includes contributions from both product N_2 and background N_2 molecules, and the red one shows the contribution from background N_2 molecules only. Apparently, the spectrum of the N_2 products is overlapped with that of the background N_2 molecules at the low J'' value region: therefore, the chamber N_2 background spectrum (red trace in Fig. 5) must be subtracted from the N_2 spectrum generated from the 5-tetrazine product N_2 spectrum (black trace in Fig. 5) in order to characterize the unique rotational distribution of N_2 product from tetrazine photodissociation (blue trace in Fig. 5). As can be seen from the blue spectrum, the major feature in the spectrum of the N_2 product from s-tetrazine is the Q(0) line.[25] This clearly indicates the N_2 product from decomposition of excited electronic state s-tetrazine exhibits a much colder rotational distribution (ca. 20 K) than the background N_2 molecule (300 K). Observation of a rotationally cold N_2 product from the decomposition of s-tetrazine excited at 202 nm can be an important indication that the triple concerted dissociation pathway is an appropriate decomposition mechanism for electronically excited s-tetrazine because this pathway does not exert a torque on the N_2 moiety as will be demonstrated below.

If the energetic tetrazine derivatives, such as ACTO and DAATO, experience a similar decomposition mechanism to that of s-tetrazine [see Fig. 2, scheme (a)], N_2O should be one of the initial products from decomposition of the excited electronic states of these molecules. Two basic options can be employed to verify this assumption: 1) direct detection of N_2O from the decomposition of ACTO and DAATO; and 2) compare the decomposition products and their internal energy distributions for N_2O gas and the tetrazine energetic derivatives. The latter approach is employed herein. Both the tetrazine based species and N_2O yield N_2 and NO at 202 nm excitation: the comparison of internal energy distributions of N_2 or NO from all three species can yield information about the decomposition of ACTO and DAATO. Assuming N_2O is produced from the photo dissociation of ACTO and DAATO, both N_2 and NO molecules should be detected as secondary decomposition products from the initial product N_2O; moreover, these detected products (N_2 or NO) should exhibit similar internal energy distributions to that of the N_2 and NO products from N_2O gas. On the other hand, if N_2O is not an initial decomposition product from these tetrazine derivatives, the N_2 and NO molecules will either not be observed, or will be detected with different internal energy distributions compared to the decomposition of N_2O gas. These detailed comparisons will determine if the three molecules tetrazine, ACTO, and DAATO decompose through similar or different reaction channels.

The (2+1) REMPI spectrum of N_2 product from decomposition of excited electronic state N_2O at 203 nm is shown in Fig. 6. The spectrum is similar to that observed by Hanisco and Kummel,[26] who have determined that the maximum rotational distribution of the N_2 product from N_2O is around $J'' = 75$, indicating a rotational temperature of greater than 2000 K: N_2 product from N_2O clearly has much hotter rotational distribution than that of room temperature, chamber N_2. The spectrum of N_2 product from N_2O is red-shifted away from that of the background N_2 molecules, and the rotational temperature of the decomposition product can be directly determined based on two photon absorption line strength and Boltzmann population distribution.[25] Therefore, if N_2O is produced from the decomposition of tetrazine derivatives, the

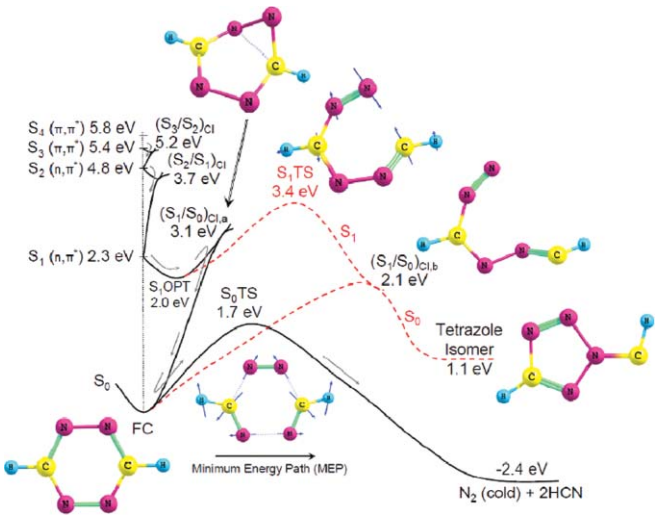

FIG. 7. PESs of s-tetrazine obtained at a CASSCF(14, 11)/6–31G(d) theory level. Two pathways are possible following electronic excitation of this molecule at 203 nm: (1) internal conversion to the ground state through a half chair form of tetrazine ring followed by concerted triple dissociation producing rotationally cold N_2 and (2) C-N bond dissociation on the S_1 surface followed by nonadiabatic transition to S_0 on which an isomeric tetrazole derivative is formed. Arrows in the figure indicate the minimum energy pathway. Energies associated with the S_1 excited state are scaled by 0.7. Note that the N_2 molecule gets almost no torque along the S_0 dissociation MEP.

secondary decomposition product N_2 from the N_2O intermediate should be detected without the interference from background N_2 inside the chamber. After considerable searching in the wavelength range 202 to 205 nm, no N_2 product has been observed from decomposition of excited electronic state ACTO and DAATO at these excitations. This observation indicates that the energetic tetrazine derivatives decompose along pathways different from that of the unsubstituted tetrazine ring; thus, N_2O is not an initial decomposition product from ACTO and DAATO. This observation also implies that the substituent groups on the tetrazine ring significantly change the potential energy surfaces of the tetrazine system, which enables a different decomposition pathway.

Instead of N_2 or N_2O as a dissociation product from decomposition of excited electronic state ACTO and DAATO, NO is observed as an initial decomposition product with hot vibrational (1200 K) and cold rotational distributions following excitation at 226, 236 and 248 nm.[22] Moreover, only the (0–0) vibronic band of the NO product is observed from photolysis of N_2O at 226 nm photoexcitation, and the spectrum is characterized by a rotational temperature of about 150 K.[22] Assuming N_2O is an intermediate precursor for the NO product in the decomposition of excited electronic state energetic tetrazine derivatives, the final NO product should present similar or hotter rotational or vibrational distributions compared to that from N_2O gas, which is cooled before photolysis under molecular beam conditions. NO from photolysis of $DAATO_{3,5}$ and ACTO is, however, rotationally colder and vibrationally hotter than that from N_2O gas. These differences indicate that N_2O cannot be an intermediate precursor for the NO product in the decomposition of excited electronic state energetic tetrazine derivatives. Instead, a ring contraction mechanism (see Sec. V and Fig. 2) is proposed to be the mechanism of NO elimination from these molecules. Furthermore, one can also infer that excited electronic state decomposition behavior of energetic tetrazine derivatives is essentially different from that of unsubstituted s-tetrazine.

V. THEORETICAL RESULTS

To assess which excited electronic state of s-tetrazine is prepared by 202 nm excitation, a comparison between the computed vertical excitation energies and experimental excitation energy is performed. The calculations are performed at the CASSCF/6–31G(d) level of theory with an active space comprising 14 electrons and 11 orbitals. As shown in Fig. 7, the vertical excitation energies of the four lowest lying excited electronic states (S_1, S_2, and S_3, and S_4) of s-tetrazine are calculated to be 3.3, 4.8, 5.4, and 5.8 eV, respectively.

The absorption spectrum of s-tetrazine has been studied in detail over many decades. Figure 8 shows an absorption spectrum of s-tetrazine vapor in the energy range of 2.1–6.1 eV (590–202 nm).[2] It displays well resolved vibronic band peaks associated with the ($\pi^* \leftarrow$ n) electronic transition in the visible wavelength range of 440–590 nm (2.8–2.1 eV). No absorption occurs in the range of 280–440 nm (4.43–2.8 eV). The UV absorption spectrum of s-tetrazine shows a diffuse band extending from 4.43 eV (280 nm) to the deep UV region (202 nm) with a maximum at 5.0 eV (247 nm). This diffuse band arises due to ($\pi^* \leftarrow \pi$) electronic transitions of the s-tetrazine molecule. Therefore, the calculated vertical excitation energies of the S_2, S_3, and S_4 states of s-tetrazine are in good agreement with the experimental UV absorption spectrum of this molecule. The calculated vertical excitation energy (3.3 eV) of the S_1 state, however, which arises due to ($\pi^* \leftarrow$ n)

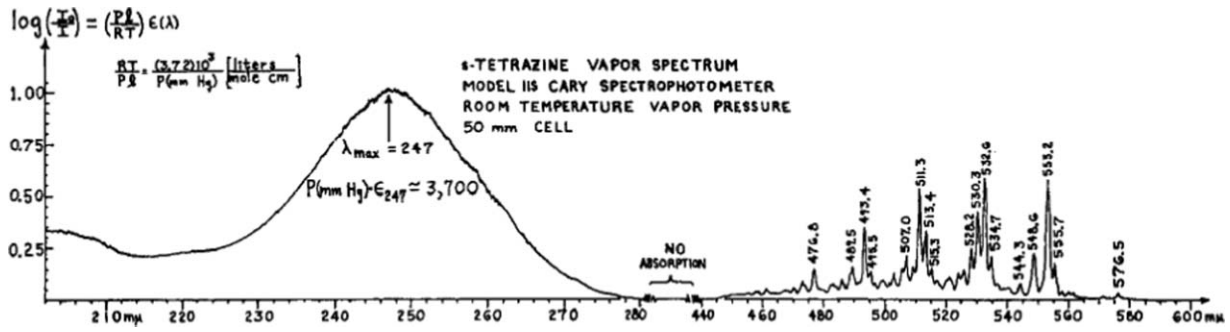

FIG. 8. Absorption spectrum of s-tetrazine vapor at room temperature measured by Spencer *et al.* (Ref. 2).

electronic transition of s-tetrazine, is in poor agreement with the experimental absorption maximum of 2.3 eV, even at the MP2 correlated CASSCF level of theory (3.4 eV). In order to compare the vertical excitation energy and the energies of the critical points on the S_1 surface of s-tetrazine with its visible absorption spectrum, a scaling factor of 0.7 (2.3/3.3) is used. This helps us evaluate the reaction path that is involved in the decomposition of excited electronic state s-tetrazine. Based on a comparison of the experimental absorption spectrum and the calculated vertical excitation energies of s-tetrazine, one can infer that s-tetrazine is excited to its S_4 electronic excited state by 202 nm excitation.

A schematic one-dimensional projection of the multidimensional singlet potential energy surfaces (S_0, S_1, S_2, S_3, and S_4) of s-tetrazine with locations and structures for different critical points and conical intersections, is plotted in Fig. 7. The plot shows that following vertical excitation to the FC point of the S_4 surface, s-tetrazine can undergo rapid nonadiabatic internal conversion from S_4 to S_3 to S_2, and finally to S_1 through the $(S_4/S_3)_{CI}$ (not shown in the figure), $(S_3/S_2)_{CI}$, and $(S_2/S_1)_{CI}$ conical intersections sequentially. Other possible conversion paths, such as S_4 directly to S_0 or S_4 to S_2, cannot be completely excluded in this work. Nevertheless, because of the availability of conical intersections between neighboring excited electronic state adiabatic PESs with small energy separations, and thereby strong nonadiabatic coupling between them, we propose that the S_4 state relaxes back to the S_1 surface nonradiatively through all neighboring conical intersections. These nonadiabatic internal conversions occur without significant change in nuclear configuration (molecular geometry), and are energetically viable from the FC point of the S_4 surface because no barrier exists along the minimum energy pathway (MEP, steepest pathway) for these processes.

Following internal conversion to the S_1 surface, under isolated molecular beam conditions, the excitation energy is stored in the vibrational degrees of freedom of s-tetrazine on the S_1 surface. A ring opening process on the S_1 surface is calculated to possess an activation barrier of 3.4 eV with respect to the S_0 FC point (see Fig. 7). An $(S_1/S_0)_{CI,a}$ conical intersection with a half chair ring geometry for s-tetrazine is predicted to have an activation energy barrier of 3.1 eV with respect to the S_0 FC point. Therefore, s-tetrazine can easily follow the minimum energy pathway along $(S_1/S_0)_{CI,a}$ and can come back to the ground state with considerable vibrational excitation. On the S_0 surface a concerted triple dissociation of tetrazine ring can take place which can produce rotationally cold N_2 molecules. The activation barrier for this concerted triple dissociation of tetrazine is predicted to be 1.7 eV which can easily be surmounted by the stored energy (6.14 eV at 202 nm excitation) in its vibrational degrees of freedom on its ground electronic state surface. Thereby, in brief, s-tetrazine can dissociate through concerted triple dissociation pathway on the ground state surface after a series of internal conversions to the ground state from excited electronic states following electronic excitation at 202 nm. Note that little torque is generated on the N_2 dissociating molecule in this dissociation coordinate.

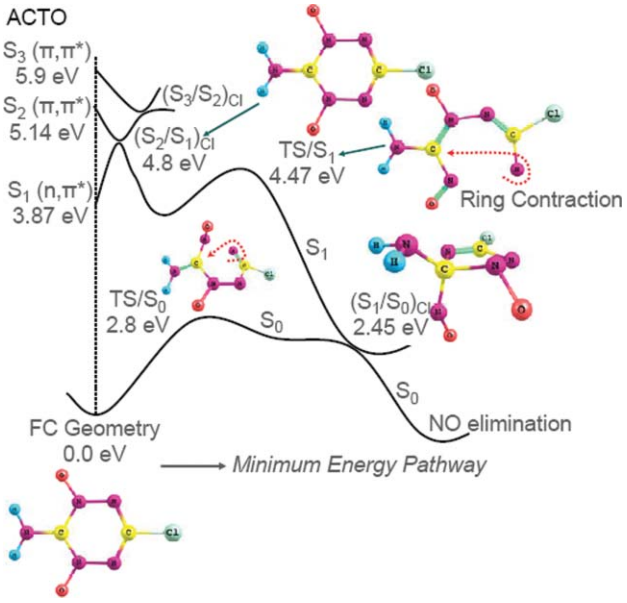

FIG. 9. One dimensional projection of the multidimensional singlet electronic potential energy surfaces of ACTO computed at CASSCF(10, 8)/6–31G(d) theory level. Geometry near the $(S_1/S_0)_{CI}$ supports a ring contraction mechanism for decomposition of excited electronic state ACTO, which finally results in NO elimination on S_0. Note that a ring contracted form of ACTO near the $(S_1/S_0)_{CI}$ has nearly linear C-NO moiety attached to the triazole ring, which can finally generate a rotationally cold NO product.

Detailed CASSCF calculational results for ACTO have been published in our previous paper.[22] Only a brief summary is provided here for comparison purposes. The CASSCF calculations show that the three lowest lying excited electronic states (S_1, S_2, and S_3 in Fig. 9) for ACTO have vertical excitation energies of 3.87, 5.14, and 5.9 eV, respectively. Comparison of the experimental excitation energies (5.5 eV at 226 nm, 5.26 eV at 236 nm, and 5.00 eV at 248 nm) used in this work with the calculated vertical excitation energies at the MP2 correlated CASSCF level of theory indicates that these UV-photoexcitation of ACTO primarily populate the Franck-Condon modes of the S_3 or S_2 surface. A schematic one-dimensional projection of the multidimensional singlet potential energy surfaces (S_0, S_1, S_2, and S_3) of ACTO with locations and structures of different critical points and conical intersections following the ring contraction pathway is plotted in Fig. 9. Similar to s-tetrazine, following vertical excitation to the FC point of the S_3 surface, ACTO can undergo rapid nonadiabatic internal conversion from S_3 to S_2 through the $(S_3/S_2)_{CI}$ and thereafter, from S_2 to S_1 through the $(S_2/S_1)_{CI}$ conical intersection. These nonadiabatic state changes occur without significant change in nuclear configuration (molecular geometry). These processes are energetically viable from the FC point of the S_3 surface, because practically no barriers exist along the minimum energy pathway (MEP) for these processes.

Following internal conversion to the S_1 surface, under isolated molecular beam conditions, the excitation energy is stored in the vibrational degrees of freedom of the molecule on the S_1 surface. Therefore, a ring contraction excited electronic state process can be initiated on the S_1 surface of ACTO. On the S_1 surface, the activation barrier (at 4.47 eV with respect to the S_0 FC point, see Fig. 9) for ring contraction

of ACTO can easily be surmounted because the excess energy stored in the vibrational degrees of freedom of the S_1 molecule, following radiationless internal conversion of the ACTO to the S_1 surface, is sufficient to surmount the barrier. Following this transition state, the molecule is directed to $(S_1/S_0)_{CI}$ and relaxes back to the S_0 surface upon which NO elimination takes place with no activation barrier. Thereby, in brief, the ring contraction of the electronically excited ACTO, which leads to the formation of ground state NO as an initial decomposition product, begins on the S_1 surface and develops through the $(S_1/S_0)_{CI}$. The mechanism generates a rotationally cold NO.

VI. DISCUSSION

Theoretical results (see Fig. 7) show that a concerted triple dissociation of the s-tetrazine ring is involved in the production of N_2 product from decomposition of excited state s-tetrazine. Following single photon absorption at 202 nm, the s-tetrazine molecule is excited to its S_4 electronic state, then relaxes back to the S_1 surface through (S_4/S_3), $(S_3/S_2)_{CI}$, and $(S_2/S_1)_{CI}$ conical intersections sequentially with high vibrational excitation. Following internal conversion to the S_1 surface, s-tetrazine can either experience a ring opening process on the S_1 surface to form a tetrazole isomer on the S_0 surface after passing through the $(S_1/S_0)_{CI,b}$ conical intersection, or relax back to the S_0 surface through the $(S_1/S_0)_{CI,a}$ conical intersection with a half chair ring geometry. The activation energy barriers for the ring opening process and the internal conversion through the $(S_1/S_0)_{CI,a}$ conical intersection are 3.4 and 3.1 eV, respectively, with respect to the S_0 FC point. Therefore, we suggest that the s-tetrazine molecule returns to the ground electronic state with high vibrational excitation following the minimum energy pathway along the $(S_1/S_0)_{CI,a}$ conical intersection, and experiences a concerted, triple dissociation on the S_0 surface to produce N_2 and HCN as decomposition products. Compared to the activation energy barrier (1.7 eV) for the concerted triple dissociation of s-tetrazine, the excitation energy in this work (6.1 eV at 202 nm) is large enough to surmount the barrier. More importantly, this concerted triple dissociation mechanism will produce the N_2 molecule without any torque, which leads to a cold rotational distribution for the N_2 product from decomposition of excited state s-tetrazine. This is consistent with the experimental observation, and is in a good agreement with Zhao *et al.*[10]

For ACTO and DAATO, on the other hand, no N_2 product has been observed from the decomposition of excited state tetrazine energetic derivatives at 202 nm excitation. Instead, an NO product has been observed as an initial decomposition product with cold rotational (20 K) and hot vibrational (1200 K) distributions. A concerted triple dissociation of the tetrazine ring would produce N_2O as an initial product from ACTO and DAATO based on Fig. 2(a), assuming that the tetrazine energetic derivatives experience a similar decomposition pathway to that of s-tetrazine itself. As mentioned in Sec. IV, comparison of the decomposition products and their internal energy distributions for N_2O gas and the tetrazine energetic derivatives can test this assumption.

Excitation of N_2O gas at 203 nm generates both N_2 and NO decomposition products: N_2 is generated rotationally hot (∼2000 K) in this process and NO is generated with a hot (∼150 K) rotational distribution and a cold vibrational (0-0 only) distribution. This energy partition is very different from that observed for NO from ACTO and DAATO. Therefore, one can exclude N_2O as the intermediate precursor of the NO product from ACTO and DAATO. Moreover, one can conclude that N_2O should not be an initial product from decomposition of excited electronic state tetrazine energetic derivatives. These results indicate that decomposition of excited electronic state tetrazine energetic derivatives evolves through a different mechanism from that of the unsubstituted s-tetrazine, which is confirmed to decompose through a concerted triple dissociation mechanism leading to N_2 elimination.

Theoretical results for ACTO (see Fig. 9) show that a ring contraction mechanism [Fig. 2(b)] is involved in generation of an NO product from decomposition of excited electronic state ACTO. Ring contraction takes place near the $(S_1/S_0)_{CI}$ conical intersection as the ACTO molecule evolves from low lying excited electronic states. As shown in Fig. 9, the ring contracted form of ACTO near $(S_1/S_0)_{CI}$ has a nearly linear C-NO moiety (<CNO∼150°) attached to the triazole ring, which exerts minimal torque on the terminal NO moiety during the NO elimination process, and can finally generate a rotationally cold NO product, which is consistent with experimental observations. In addition, comparison between the potential energy surfaces of s-tetrazine (Fig. 7) and ACTO (Fig. 9) shows that the substituents (NH_2, Cl atom, and O atom) on the tetrazine ring significantly modify the potential energy surfaces of the unsubstituted tetrazine, thus leading to a different decomposition pathway to produce different products with different internal energy distributions. Decomposition products and internal energy distributions in these products are important parameters for the quality, performance, and sensitivity of these energetic derivatives as fuels and explosives. Therefore, by modifying the substituents on the root molecule (tetrazine in this case), and analyzing the decomposition products and internal energy distributions, one can obtain useful information for improvement and control of new energetic materials.

Due to the wavelength limitation, only the (0–0) rovibronic transitions of the N_2 product from decomposition of excited electronic state s-tetrazine is detected in our experiments. Nevertheless, based on the determination of the decomposition mechanism of s-tetrazine, the concerted triple dissociation pathway needs a lot of energy to break the three chemical bonds: this suggests that higher vibrational excitation of the N_2 product may not occur. For tetrazine energetic derivatives, on the other hand, the ring contraction mechanism only breaks one chemical bond to produce an NO product, therefore a large amount of extra energy will be redistributed as internal energy (in this case mostly to the vibrational degrees of freedom) of the NO product. This excitation is consistent with the experimental observation that NO from ACTO and DAATO has a hot vibrational distribution (1200 K). Based on the observations of different energetic materials (such as nitramine, furazan, and tetrazine

based systems),[16–18,22] decomposition products with hot vibrational distributions are a unique characteristic of energetic molecules. Initial decomposition products with high vibrational excitation are also more able to initiate a chain reaction following an initiation stimulus, and lead to detonation of energetic materials.

VII. CONCLUSIONS

Decomposition of excited electronic state s-tetrazine produces N_2 as an initial product with a cold rotational distribution. A concerted triple dissociation mechanism is responsible for the production of N_2 from the excited s-tetrazine molecule after fast relaxation from highly excited electronic states to the ground electronic state through a series of conical intersections. Decomposition of excited electronic state tetrazine energetic derivatives (ACTO and DAATO), on the other hand, produces NO as an initial product with cold rotational (20 K) and hot vibrational (1200 K) distributions. N_2O is a potential decomposition product from ACTO and DAATO also through a concerted triple dissociation pathway: nonetheless, N_2O is determined not to be an intermediate precursor for the observed NO product generated from decomposition of excited electronic states of these energetic derivatives of s-tetrazine. Instead, due to the modification to the potential energy surfaces of the tetrazine molecule by the N-oxide substituents, a ring contraction mechanism is found for the decomposition of excited electronic state ACTO and DAATO. This dissociation channel leads to an NO rather than an N_2 initial product from these high nitrogen content energetic systems.

ACKNOWLEDGMENTS

We gratefully thank Dr. Sumit Dey in the Chemistry Department at Colorado State University for his help in the synthesis of s-tetrazine sample. These studies are supported by a grant from US ARO.

[1] S. F. Mason, J. Chem. Soc. **1959**, 1263.
[2] G. H. Spencer, Jr., P. C. Cross, and K. B. Wiberg, J. Chem. Phys. **35**, 1925 (1961).
[3] K. K. Innes, J. P. Byrne, and I. G. Ross, J. Mol. Spectrosc. **22**, 125 (1967); K. K. Innes, I. G. Ross, and W. R. Moomaw, *ibid.* **132**, 492 (1988).
[4] D. V. Brumbaugh, C. A. Haynam, and D. H. Levy, J. Mol. Spectrosc. **94**, 316 (1982).
[5] K. B. Thakur, V. A. Job, and V. B. Kartha, J. Mol. Spectrosc. **107**, 373 (1984).
[6] A. C. Sheiner and H. F. Schaefer III, J. Chem. Phys. **87**, 3539 (1987).
[7] R. M. Hochstrasser and D. S. King, J. Am. Chem. Soc. **98**, 5443 (1976).
[8] R. M. Hochstrasser, D. S. King, and A. B. Smith, J. Am. Chem. Soc. **99**, 3923 (1977).
[9] T. J. Aartsma, W. H. Hesselink, and D. A. Wiersma, Chem. Phys. Lett. **71**, 424 (1980).
[10] X. S. Zhao, W. B. Miller, E. J. Hintsa, and Y. T. Lee, J. Chem. Phys. **90**, 5527 (1989).
[11] J. H. Meyling, R. P. Van Der Werf, and D. A. Wiersma, Chem. Phys. Lett. **28**, 364 (1974).
[12] R. M. Hochstrasser and D. S. King, Chem. Phys. **5**, 439 (1974).
[13] A. C. Scheiner, G. E. Scuseria, and H. F. Schaefer, J. Am. Chem. Soc. **108**, 8160 (1986).
[14] D. S. King, C. T. Denny, R. M. Hochstrasser, and A. B. Smith III, J. Am. Chem. Soc. **99**, 271 (1977).
[15] D. M. Burland, F. Carmona, and J. Pacansky, Chem. Phys. Lett. **56**, 221 (1978).
[16] Y. Q. Guo, M. Greenfield, and E. R. Bernstein, J. Chem. Phys. **122**, 244310 (2005).
[17] Y. Q. Guo, M. Greenfield, A. Bhattacharya, and E. R. Bernstein, J. Chem. Phys. **127**, 154301 (2007).
[18] Y. Q. Guo, A. Bhattacharya, and E. R. Bernstein, J. Chem. Phys. **128**, 034303 (2008).
[19] D. E. Chavez, M. A. Hiskey, and D. L. Naud, Propellants, Explos., Pyrotech. **29**, 209 (2004).
[20] D. E. Chavez, M. A. Hiskey, M. H. Huynh, D. L. Naud, S. F. Son, and B. C. Tappan, J. Pyrotech. **23**, 70 (2006).
[21] G. Steinhauser and T. M. Klapotke, Angew. Chem., Int. Ed. **47**, 3330 (2008).
[22] A. Bhattacharya, Y. Q. Guo, and E. R. Bernstein, J. Chem. Phys. **131**, 194304 (2009).
[23] W. L. Glab and J. P. Hessler, Appl. Opt. **26**, 3181 (1987).
[24] M. J. Frisch, G. W. Trucks, H. B. Schlegel *et al.*, GAUSSIAN03, Revision B.04, Gaussian Inc., Pittsburgh, PA, 2003.
[25] K. R. Lykke and B. D. Kay, J. Chem. Phys. **95**, 2252 (1991).
[26] T. F. Hanisco and A. C. Kummel, J. Phys. Chem. **97**, 7242 (1993).